Volume 13
Number 2
February 2020
Pages 321–650

Energy & Environmental Science

rsc.li/ees

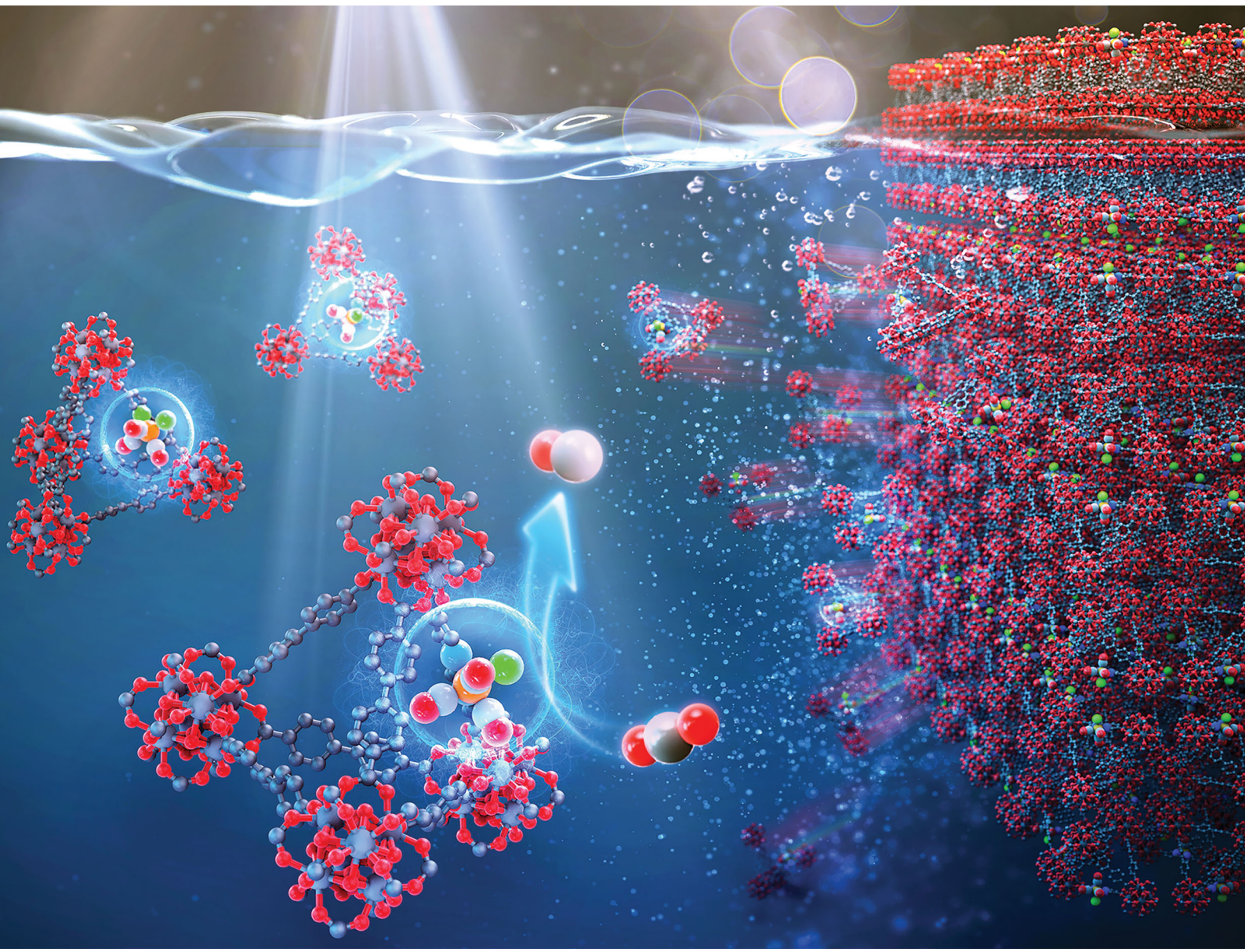

ISSN 1754-5706

ROYAL SOCIETY OF CHEMISTRY

PAPER

Wooyul Kim, Kyung Min Choi *et al.*

A highly active, robust photocatalyst heterogenized in discrete cages of metal–organic polyhedra for CO_2 reduction

Energy & Environmental Science

PAPER

View Article Online
View Journal | View Issue

Cite this: *Energy Environ. Sci.*, 2020, **13**, 519

A highly active, robust photocatalyst heterogenized in discrete cages of metal–organic polyhedra for CO_2 reduction†

Hyeon Shin Lee,[a] Seohyeon Jee,[a] Raekyung Kim,[a] Hoang-Tran Bui,[a] Bupmo Kim,[b] Jung-Keun Kim,[c] Kyo Sung Park,[c] Wonyong Choi,[b] Wooyul Kim *[a] and Kyung Min Choi *[a]

Received 14th August 2019,
Accepted 29th October 2019

DOI: 10.1039/c9ee02619c

rsc.li/ees

The heterogenization of photocatalytic molecules typically enhances stability at the expense of activity. Therefore, a new approach to stabilizing molecular catalysts without compromising their original catalytic features is highly desired. In this study, we found that Zr-based metal–organic polyhedra (MOP) stabilized the photocatalytic compound ReTC [$Re^{I}(CO)_3$(BPYDC)(Cl), BPYDC = 2,2′-bipyridine-5,5′-dicarboxylate] without degrading its catalytic activity. ReTC was chemically bound to discrete cages of the MOP and was found to maintain its maximum CO_2-to-CO conversion activity (660 h^{-1} turnover frequency (TOF)) for at least 24 h under visible light irradiation. The free molecular form of the same compound (H_2ReTC) initially showed an activity of 131 h^{-1} TOF, which was lost within 2 h. The cumulative turnover number of ReTC-MOP after a 24 h reaction was 12 847, which was 42.0 times the value of 306 for molecular ReTC. The high catalytic activity and stability of ReTC-MOP are attributed to the fact that this MOP material provides an extremely small framework for chemical binding of ReTC, such that the catalyst has a high degree of motional freedom and enhanced light absorption while being protected in the reaction solution.

Broader context

Development of highly active, selective, and long-lasting catalysts is sought-after in both heterogeneous and homogeneous catalysis. Especially, photo-active catalysts converting the green-house gas CO_2 into valuable hydrocarbon products using visible light are becoming more important to solve energy and environmental problems. Photocatalyst molecules, having powerful features of high activity and product selectivity, have challenges concerning their catalytic stability as they are easily transformed to an inactive form and not reusable. In this report, we discovered that discrete cages of metal–organic polyhedra (MOP), structured with an organic linker and inorganic joint, ultimately stabilize a molecular catalyst without loss of its original catalytic activity. The molecular catalyst chemically bound to the MOP preserved its high CO_2-to-CO conversion activity for at least 24 h under visible light irradiation and its cumulative turnover number (12 847) was 42.0 times the value for the molecular catalyst. The significant activity and stability of the MOP catalyst arise from the high degree of motional freedom, enhanced light absorption and protection of the molecular catalyst in the reaction solution.

The reduction of carbon dioxide (CO_2) with sunlight *via* artificial photosynthetic systems provides an opportunity to utilize non-arable land for the generation of renewable fuels and to reduce the atmospheric concentrations of greenhouse gases.[1–4] Recent substantial progress toward the development of more efficient light absorbers and catalysts for water oxidation and increasing interest in CO_2 activation catalysts suggest the viability of solar processes. In particular, photocatalytic CO_2 reduction systems based on metal complexes have attracted attention as a key component of artificial photosynthetic systems because of their high efficiencies and selectivities for the desired products.[5–8] The molecular nature of these metal complexes allows specific fine-tuning of their structure to rationally control both activity and selectivity. However, challenges exist regarding the stability of molecular catalysts, because they are readily transformed to non-active forms during prolonged reactions.[9,10]

[a] *Department of Chemical and Biological Engineering, Sookmyung Women's University, Seoul, 04310, Korea. E-mail: wkim@sookmyung.ac.kr, kmchoi@sookmyung.ac.kr*
[b] *Division of Environmental Science and Engineering, Pohang University of Science and Technology (POSTECH), Pohang 37673, Korea*
[c] *LG Science Park, 30, Magokjungang 10-ro, Gangseo-gu, Seoul 07796, Republic of Korea*

† Electronic supplementary information (ESI) available: Experimental details, structural scheme, characterization and supporting photocatalytic performances. See DOI: 10.1039/c9ee02619c

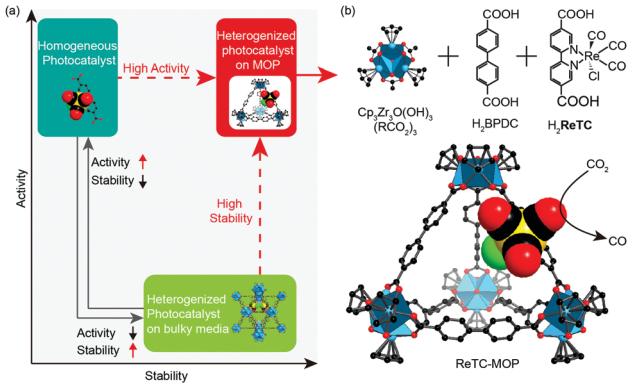

Fig. 1 Schematic diagrams showing the heterogenization of a photocatalyst on MOP. (a) The photocatalyst heterogenized on the MOP shows enhanced stability without a decrease in activity. (b) The structure of ReTC-MOP for photocatalytic CO_2-to-CO conversion. Atom labels: C, black; O, red; Zr, blue polyhedra; Re, yellow; Cl, green; H atoms are omitted.

To address these issues, homogeneous photocatalysts based on metal complexes have been chemically bound to various organic or inorganic supporting materials (known as heterogenization). These supports include various types of porous silica,[11,12] carbon,[13–15] metal nanostructures[16–23] and metal–organic frameworks (MOFs),[24–37] such that deteriorative transformations are prevented. However, this increased stability is typically achieved at the expense of decreased catalytic activities (Fig. 1). This occurs because the flexibility and accessibility of the homogeneous photocatalysts (*i.e.*, the metal complexes) are hindered upon heterogenization on bulky supporting media, thus reducing their catalytic activities.[38] Unfortunately, soft organic-based supporting media have been shown not to effectively stabilize photocatalytic molecules.[39] Consequently, a new type of rigid supporting media is urgently required to boost the stability of these complexes without degrading their intrinsic high activity and selectivity (Fig. 1).

Metal–organic polyhedra (MOP) constructed from organic linkers and inorganic joints exhibit rigid porous structures,[40,41] similar to those of the better-known MOFs. However, MOP have terminal groups on their inter-connecting sites, such that each unit cell exists independently as a discrete cage on the molecular scale (Fig. 1).[40,41] In this study, we demonstrate that MOP comprising discrete cages and containing a homogeneous photocatalyst allow the high catalytic activity of the material to be retained without decomposition during prolonged CO_2 conversion under visible light irradiation (Fig. 1). Specifically, we covalently attached $Re^{I}(CO)_3(BPYDC)(Cl)$ (BPYDC = 2,2′-bipyridine-5,5′-dicarboxylate), hereafter ReTC, to Zr-based MOP to produce a material referred to herein as ReTC-MOP (Fig. 1). After characterization of ReTC-MOP, its photocatalytic CO_2-to-CO conversion performance was assessed under visible light and compared to the performance of molecular H_2ReTC and ReTC containing MOFs with nano or microscale crystal sizes (hereafter referred to as ReTC-MOF(nano) and ReTC-MOF(micro), respectively) (Fig. S1, ESI†).[24–27] ReTC-MOP exhibited a CO-based turnover frequency (TOF_{CO}) of 660 h^{-1} for up to 24 h, while H_2ReTC initially showed a TOF_{CO} of 131 h^{-1} but lost its activity within 2 h. The cumulative turnover number (TON) of ReTC-MOP after a 24 h reaction was 12 847, which was 42.0, 19.6 and 29.3 times the values obtained from H_2ReTC, ReTC-MOF(nano) and ReTC-MOF(micro), respectively. The high activity and stability of ReTC-MOP were further studied using *in situ* ultraviolet (UV) and attenuated total reflectance (ATR) Fourier transform infrared (FT-IR) spectroscopy. The results showed that the high photocatalytic activity of ReTC-MOP can be attributed to the motional freedom of ReTC and the enhanced light absorption of this material in the reaction solution. The high stability of this catalyst was ascribed to the structural rigidity of the MOP, which maintained the molecular conformation of ReTC.

There have been reports concerning the use of bare MOP as heterogeneous catalysts or to anchor metal ions for organic, thermal and photochemical catalysis.[42–47] However, the application of MOP to the anchoring of molecular photocatalysts for CO_2 conversion has not yet been reported. In prior work, including our own, ReTC has been heterogenized on various supporting media, such as Zr-based MOFs,[24,26,27] but the original catalytic activity of ReTC has always been severely deteriorated even when the stability is enhanced. The present work is the first instance of the use of discrete cage-type MOP as a support for photocatalytic CO_2 conversion. The results of this study show that the superior activity and selectivity of the homogeneous photocatalyst are preserved even after heterogenization for higher stability.

Zr-based MOP were chosen because this material is chemically stable under photocatalytic conditions, and a 4,4′-biphenyldicarboxylate (BPDC) linker was used to produce the basal construct of the MOP (BPDC-MOP) (Fig. S1a, ESI†).[48–50] In the BPDC-MOP structure, each Zr cluster ($[Cp_3Zr_3O(OH)_3(CO_2)_3]^+$) at a vertex is connected to three BPDC units to form a porous tetrahedral cage (Fig. S1a, ESI†). ReTC-MOP was designed such that a ReTC unit was substituted for one of the BPDC units within the BPDC-MOP cage (Fig. 1 and Fig. S1b, ESI†). The conditions for the synthesis of both ReTC- and BPDC-MOP were identical, except that the protonated form H_2ReTC (17 mol%) was mixed with protonated H_2BPDC (83 mol%) in the solution used to prepare ReTC-MOP. These two linkers were dissolved together with bis(cyclopentadienyl)zirconium dichloride (Cp_2ZrCl_2) in a mixture of *N*,*N*-dimethylacetamide (DMA) and deionized (DI) water, followed by heating at 85 °C for 16 h to give cubic crystals of ReTC- and BPDC-MOP (Fig. 2 and Fig. S2, ESI†). These crystals formed *via* the periodic arrangement of MOP cages based on hydrogen bonding between Cl^- ions and μ_2-OH groups in the Zr clusters.[45] When these crystals were immersed in methanol, the ReTC- and BPDC-MOP cages were unpacked as a result of the disruption of hydrogen bonding and the resulting species were well dispersed as separated particulates (Fig. 3 and Fig. S3, ESI†). These discrete cages were collected by centrifugation at 8000 rpm for 10 min and then dried under a vacuum. ReTC- and BPDC-MOP crystals were characterized by scanning transmission electron microscopy (STEM), energy-dispersive X-ray spectroscopy (EDX) and powder X-ray diffraction (PXRD) to

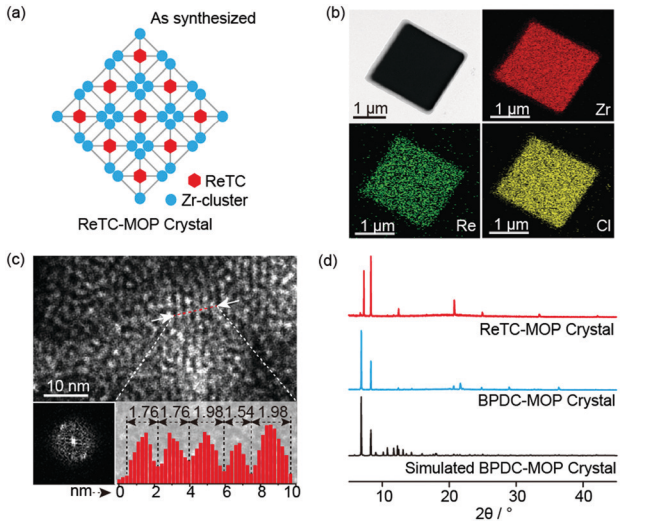

Fig. 2 Crystals of ReTC-MOP and BPDC-MOP. (a) A schematic of an ReTC-MOP crystal, (b) a STEM image and EDX results for an ReTC-MOP crystal, (c) a STEM image of ReTC-MOP in the crystal, a Fourier-transformed image of the ReTC-MOP crystal (bottom-left) and a cage size profile of ReTC-MOP (bottom-right), and (d) PXRD patterns of ReTC-MOP and BPDC-MOP crystals compared to a simulated pattern for BPDC-MOP.

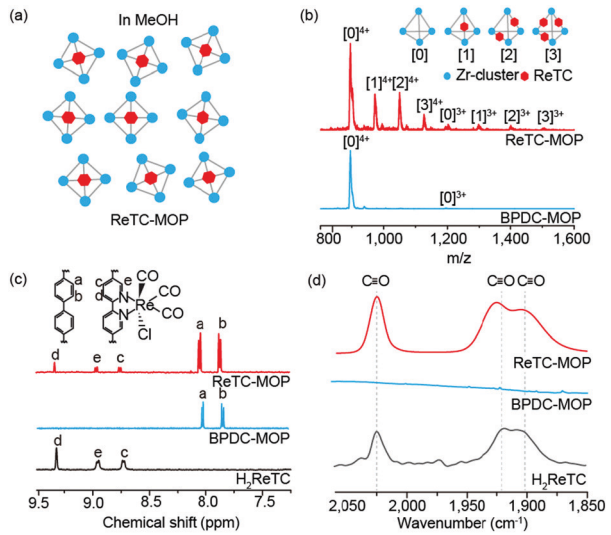

Fig. 3 Discrete cages of ReTC-MOP and BPDC-MOP. (a) A schematic of the ReTC-MOP cages, (b) ESI mass spectra of ReTC-MOP and BPDC-MOP (inset: four types of ReTC-MOP cages with different numbers of ReTC linkers; [X] = number of ReTC linkers), (c) ^{1}H NMR spectra of ReTC-MOP, BPDC-MOP and H_2ReTC and (d) IR spectra of ReTC-MOP, BPDC-MOP and of well-dispersed H_2ReTC.

elucidate their morphologies, compositions and crystal structures, respectively. The ReTC- and BPDC-MOP cages were characterized by electrospray ionization (ESI) mass spectrometry (MS), ^{1}H nuclear magnetic resonance (NMR) spectroscopy, inductively coupled plasma atomic emission spectroscopy (ICP-AES), N_2 sorption analysis and infrared (IR) and ultraviolet-visible (UV) spectroscopy, to determine their structures, compositions, porosities, and molecular configurations, respectively.

The ReTC- and BPDC-MOP crystals were observed by STEM, and Fig. 2b and Fig. S2 (ESI†), respectively, provide representative images. Both materials were composed of cubic crystals as a result of their cubic unit cells comprising eight tetrahedral MOP cages packed at each octant position (Fig. S2, ESI†).[45] The EDX mapping image (Fig. 2b) confirms that both Re and Cl were distributed throughout the ReTC-MOP crystal, while these elements were not found in the BPDC-MOP crystal (Fig. S2, ESI†). These results indicate that the ReTC units were present in the majority of the ReTC-MOP cages comprising the crystals. The ReTC-MOP crystals were also examined using STEM to elucidate the periodic arrangement and the size of the ReTC-MOP cages. The STEM image in Fig. 2c shows that the ReTC-MOP cages (the white spheres) were closely packed and arranged in a periodic order, which is also supported by the dots in the Fourier-transformed image (bottom-left inset of Fig. 2c). The size of the ReTC-MOP cages was measured using the contrast profile of the line indicated in Fig. 2c and was found to be 1.8 nm on average (bottom-right inset of Fig. 2c). The ReTC- and BPDC-MOP crystals were also examined by PXRD (Fig. 2d), which gave sharp diffraction lines, indicating the high crystallinity of the samples. The diffraction lines generated by the BPDC-MOP crystal were a good match to those in a simulated pattern based on a model structure (Fig. S1a, ESI†) and also similar to those obtained from the ReTC-MOP crystal. The presence of the ReTC units shifted the diffraction lines based on changes in the distances between the cages, but the basal structure of the material was the same as that of BPDC-MOP.

Each MOP cage was originally periodically packed in the crystal but these cages were disassembled and dispersed when the solvent was exchanged with methanol (Fig. 3a and Fig. S3, ESI†). The mass-to-charge (m/z) ratios of the ReTC- and BPDC-MOP cages were determined by ESI-MS (Fig. 3b). The peaks produced by the BPDC-MOP cages were at m/z values of 895.64 and 1195.53, corresponding to intact $[\mathbf{0}]^{4+}$ and $[\mathbf{0}]^{3+}$ cages, respectively (where **0** is a BPDC-MOP cage without Cl^- ions). The ReTC-MOP cages generated peaks at m/z of 895.64, 972.73, 1050.10, 1126.49, 1195.53, 1296.61, 1401.12 and 1502.60, corresponding to $[\mathbf{0}]^{4+}$, $[\mathbf{1}]^{4+}$, $[\mathbf{2}]^{4+}$, $[\mathbf{3}]^{4+}$, $[\mathbf{0}]^{3+}$, $[\mathbf{1}]^{3+}$, $[\mathbf{2}]^{3+}$ and $[\mathbf{3}]^{3+}$, respectively (where **1**, **2** and **3** are ReTC-MOP having one, two and three ReTC units, respectively). The average number of ReTC molecules per cage was confirmed by acquiring the ^{1}H NMR spectrum of ReTC-MOP following digestion in HF (Fig. 3c). Integration of the peaks in this spectrum demonstrated that 0.9 ReTC units were present in each tetrahedral cage of ReTC-MOP on average, in agreement with the value calculated from the ratio of Zr to Re concentrations determined from the ICP-AES elemental analysis. The permanent porosities of both ReTC- and BPDC-MOP were ascertained by acquiring N_2 gas adsorption isotherms (Fig. S4, ESI†). Both materials exhibited similar Type I behaviours. The amount of N_2 sorption by ReTC-MOP was slightly lower than that for BPDC-MOP because of the mass contribution by ReTC. Additional N_2 uptake at high P/P_0 values was also evident based on sorption in the inter-particle spaces in ReTC- and BPDC-MOP. The molecular configuration of ReTC was confirmed

by IR, UV-vis and NMR spectra. The IR spectrum of ReTC-MOP in powder form was obtained and ν(CO) bands were observed at 2022, 1920 and 1910 cm^{-1}, consistent with the *fac*-isomer of molecular H_2ReTC (Fig. 3d).[7] The UV-vis spectra of both ReTC-MOP and H_2ReTC contained a metal-to-ligand charge transfer (MLCT) absorption band at 400 nm (Fig. S5, ESI†), also indicative of the presence of the *fac*-isomer of ReTC.[7] This finding supported the results obtained from the ^{1}H NMR spectra shown in Fig. 3c. In contrast, BPDC-MOP did not generate any signals associated with ReTC units in either its NMR or IR spectra (Fig. 3c and d).

Samples of H_2ReTC, BPDC-MOP and ReTC-MOP were applied to photocatalytic CO_2-to-CO conversion under visible light irradiation ($\lambda > 420$ nm). Each sample containing unit was dispersed in an acetonitrile/triethylamine mixture (MeCN/TEA = 20 : 1 (v/v)) saturated with CO_2, with TEA serving as a sacrificial electron donor (Fig. S6, ESI†). The photocatalytic CO_2-to-CO conversions obtained from H_2ReTC and ReTC-MOP at the same molar amount (0.24 μmol) of ReTC units are shown in Fig. 4a. H_2ReTC was active over a span of 2 h (131 h^{-1} TOF) and then rapidly deactivated, possibly due to dimerization or decomposition as has been previously reported.[8–10] ReTC-MOP was steadily active and maintained its maximum activity (660 h^{-1} TOF) for up to 24 h (inset to Fig. 4a). The cumulative TON exhibited by ReTC-MOP confirms the highly stable photocatalytic performance throughout the entire period, with a value of 12 847 after 24 h (Fig. 4a). This value is 42.0 times higher than the result of the 306 TON obtained from H_2ReTC. No CO was produced in the absence of CO_2, TEA or light irradiation (Table 1), while other potential by-products (*i.e.* H_2, CH_4, HCOOH and CH_3OH) that could possibly be generated along with CO were not found (Fig. S7, ESI†). In additional trials, H_2ReTC was also tested at double the original amount (0.50 μmol) but the cumulative TON of 847 was still not comparable to the value for ReTC-MOP (Fig. S8, ESI† and Table 1). Even in the presence of BPDC-MOP, the cumulative TON of 290 obtained from H_2ReTC was relatively unchanged (Fig. S8 (ESI†) and Table 1). A diester form of ReTC (CH_2CH_3ReTC) was also synthesized and applied to the photocatalytic conversion because it was possible that the free carboxylic acid in H_2ReTC might affect its catalytic activity. The ^{1}H NMR spectrum of CH_2CH_3ReTC is shown in Fig. S9 (ESI†). However, the cumulative TON for CH_2CH_3ReTC was only 197 (Fig. S8 (ESI†) and Table 1), and so was much less than that for ReTC-MOP. Finally, in the case of BPDC-MOP, photocatalytic CO_2 conversion was not observed (Fig. 4a). These results imply that the ReTC units supported by the MOP were responsible for the CO production. A series of control experiments established the key properties of this photocatalytic system consisting of ReTC as the light absorber and catalyst and MOP as the supporting media to prevent the deterioration of the ReTC.

To further examine the unique properties of the MOP as a support for ReTC, we synthesized ReTC-MOF so as to produce different particle sizes on the nano and micro scales. The sizes of the ReTC-MOF crystals were controlled such that they were approximately 400 nm and 40 μm in the ReTC-MOF(nano) and ReTC-MOF(micro) products, respectively (Fig. S10, ESI†).

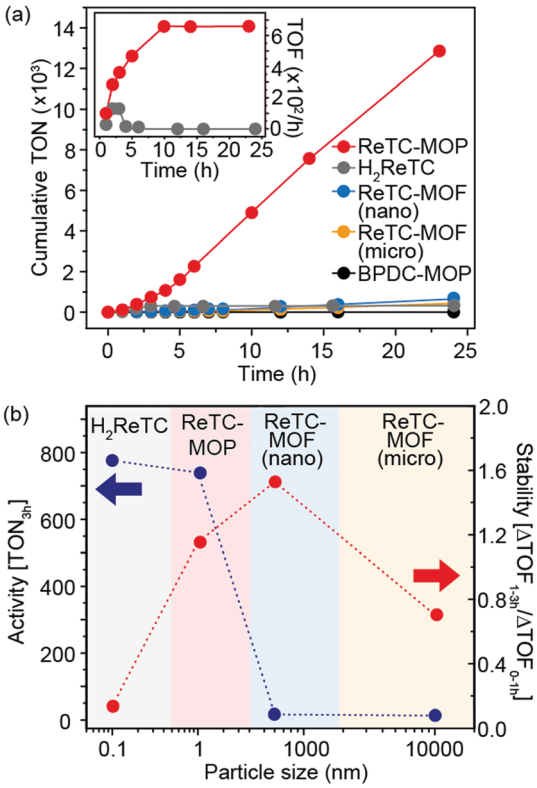

Fig. 4 Photocatalytic CO_2–CO conversion activities using various photocatalysts. (a) Cumulative TON ($\times 10^3$) values of the photocatalysts over 24 h (inset: TON ($\times 10^2$) h^{-1} of ReTC-MOP (red) and H_2ReTC (grey)). (b) Activity (TON_{3h}) and stability ($\Delta TOF_{1-3h}/\Delta TOF_{0-1h}$) trends according to the particle sizes of the photocatalysts.

The photocatalytic activities of these new materials were compared to those of H_2ReTC and ReTC-MOP (Fig. 4a). Both ReTC-MOF(nano) and ReTC-MOF(micro) showed stable photocatalytic performances (Fig. 4a), but their average TOF values were low at 27 and 18 h^{-1}, respectively (Table 1). The activities and stabilities of H_2ReTC, ReTC-MOP, ReTC-MOF(nano) and ReTC-MOF(micro) are compared in Fig. 4b. The stability of each was determined by dividing the activity over the final two h (ΔTOF_{1-3h}) by that over the initial one h (ΔTOF_{0-1h}), while the activities were directly compared based on the first three h (TON_{3h}). In this comparison, the activity of H_2ReTC when using 0.50 μmol was employed, as the activity was otherwise too small to be evaluated. Compared to the H_2ReTC and ReTC-MOF materials, which showed either high activity or high stability but not both, ReTC-MOP exhibited both increased activity and stability during photocatalytic CO_2 conversion (Fig. 4). H_2ReTC had high activity and low stability, while both ReTC-MOF materials showed low activities and high stabilities. The larger crystals of ReTC-MOF(micro), which exhibited the longest activation period, seemed to have relatively low stability in this manner of comparison, but were stable for up to 24 h in practice (albeit with the lowest activity). The observation that ReTC-MOF(micro) had lower activity and a longer activation time compared to ReTC-MOF(nano) can possibly be ascribed to the longer pathway that CO_2 and CO must migrate through

Table 1 Samples and measurement conditions for photocatalytic tests and the associated CO_2-to-CO conversions

Sample	Measurement condition	Amount of ReTC (μmol)	Total reaction time (h)	Cumulative TON_{CO}	Average TOF_{CO} (h^{-1})	Max. TOF_{CO} (h^{-1})
ReTC-MOP	Std[a]	0.24	24	12 847	558	660 from 10 h
	w/o TEA	0.24	24	N/A[b]	N/A[b]	N/A[b]
	w/o CO_2	0.24	24	N/A[b]	N/A[b]	N/A[b]
	w/o light	0.24	24	N/A[b]	N/A[b]	N/A[b]
BPDC-MOP	Std[a]	N/A	24	N/A[b]	N/A[b]	N/A[b]
H_2ReTC	Std[a]	0.24	24	306	12	131 at 2 h
	Std[a]	0.50	24	847	35	410 at 2 h
BPDC-MOP + H_2ReTC	Std[a]	0.24	24	290	12	201 at 5 h
CH_2CH_3ReTC	Std[a]	0.24	24	197	8	54 at 7 h
ReTC-MOF(nano)	Std[a]	0.24	24	654	27	36 from 13 h
ReTC-MOF(micro)	Std[a]	0.24	24	438	18	24 from 9 h

[a] Standard measurement conditions for photocatalytic conversion using an acetonitrile/TEA mixture saturated with CO_2 under visible light irradiation ($\lambda > 420$ nm). [b] A negligible amount of CO was found by GC analysis, equal to the background amount.

when using this material, as well as the sterically hindered reaction environment and the limited supply of TEA as a sacrificial electron donor.

These results imply that this MOP material represents the smallest supporting medium yet applied to catalysis, having an atomically defined framework and allowing chemical anchoring of homogeneous photocatalysts. The small size (1.8 nm) of the ReTC-MOP particles allows ready dispersion in the reaction solution and provides ReTC with the motional freedom required for photocatalysis. We propose that the ReTC molecules bound to the MOP have improved access to reactants, the flexibility to carry out the catalytic cycle and the freedom to interact with other reaction components (*i.e.* the TEA serving as the electron donor). All these effects contribute to providing high catalytic activity. Binding of the molecular catalyst to the MOP also prevents transformation of ReTC to inactive forms due to the rigid framework of the MOP, resulting in high stability. On this basis, we believe that this approach using MOP as a covalently bound support could be further extended to other functional molecules to stabilize such compounds without compromising their activities.

The photocatalytic performance of ReTC-MOP was further tested by varying the irradiation wavelength using cut-off filters (*i.e.*, $\lambda > 320$, 420, 495 and 550 nm). The amounts of CO produced after 3 h were compared. Fig. 5a shows that the photocatalytic CO_2 conversion obtained from ReTC-MOP at different wavelengths was in good agreement with its UV adsorption spectrum, indicating that the activity originated solely from ReTC-MOP. To confirm that CO was generated from the reduction of CO_2 (rather than from the degradation of other components such as electron donors, solvents, catalysts and impurities), isotope experiments were carried out using and comparing $^{13}CO_2$ and $^{12}CO_2$ as reactants (Fig. 5b). After saturating the reaction solution with $^{13}CO_2$, the ^{13}CO produced under visible light irradiation was confirmed by gas-phase FT-IR spectroscopy, using a Schlenk flask and a gas cell of our own design having CaF_2 windows. The FT-IR spectra were recorded after 10 h at a resolution of 0.25 cm^{-1} and summing 100 scans (Fig. 5b). The same experiment was also conducted using $^{12}CO_2$ as a reference. The rotational–vibrational

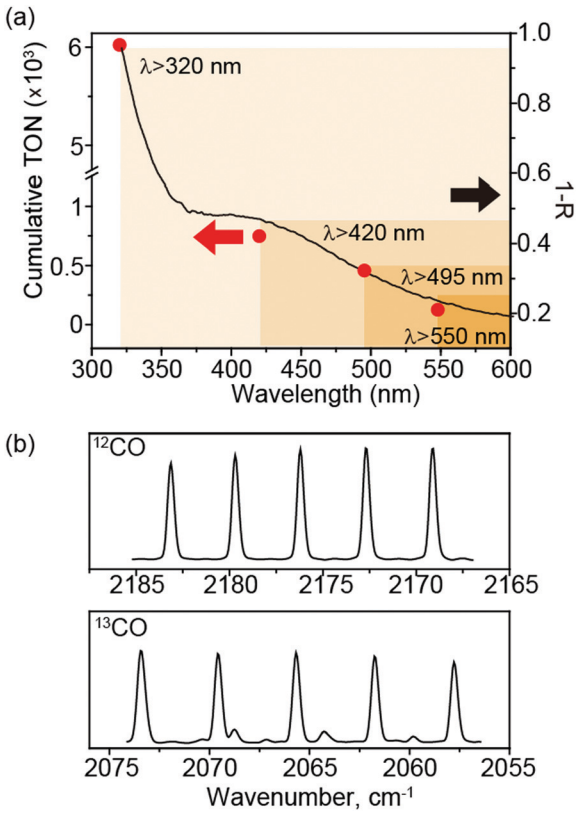

Fig. 5 Analyses finding the origin and source of the photocatalytic performance of ReTC-MOP. (a) Cumulative TON of ReTC-MOP as a function of wavelength. (b) Gas-phase FT-IR spectra of ^{12}CO (top) and ^{13}CO (bottom) produced photocatalytically from $^{12}CO_2$ and $^{13}CO_2$, respectively, using ReTC-MOP (recorded at 0.25 cm^{-1} resolution).

bands for the ^{13}CO produced from $^{13}CO_2$ appeared in the wavenumber range from 2075 to 2055 cm^{-1}, while those for ^{12}CO produced from $^{12}CO_2$ appeared from 2185 to 2165 cm^{-1} (Fig. 5b). The results indicate that both ^{13}CO and ^{12}CO primarily originated from the incoming $^{13}CO_2$ and $^{12}CO_2$, respectively.

The factors that provide ReTC-MOP with high activity and stability were investigated based on the light absorbance and structural stability. The light absorbances of ReTC units bound

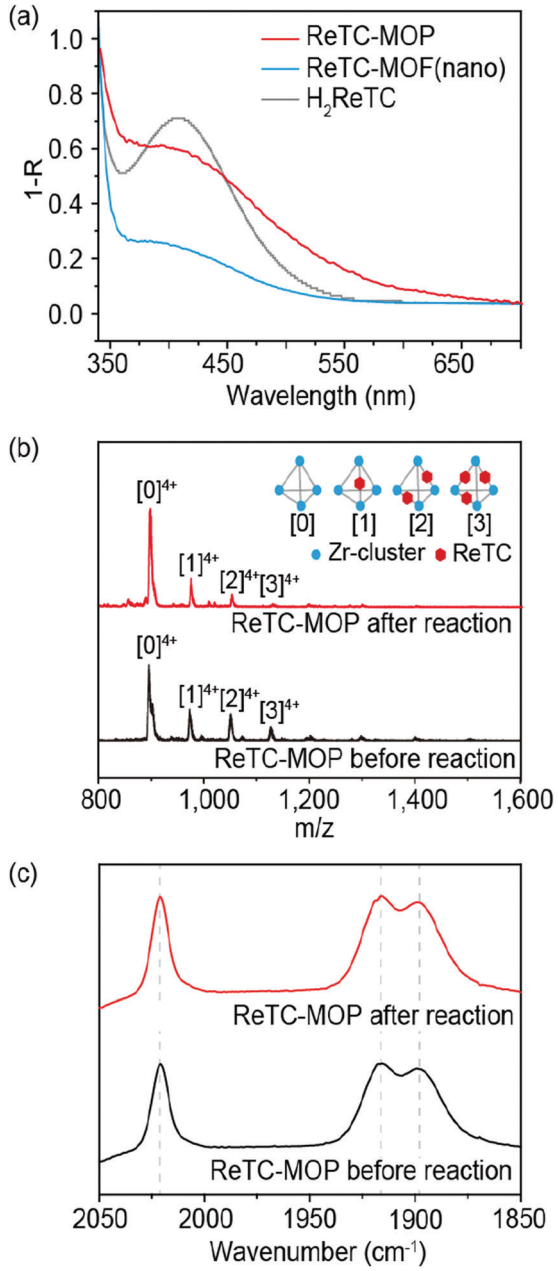

Fig. 6 Analyses explaining the high photocatalytic performance of ReTC-MOP. (a) UV-vis spectra of H_2ReTC, ReTC-MOF(nano) and ReTC-MOP. (b) ESI-MS data for ReTC-MOP before (top) and after the reaction (bottom). (c) *In situ* ATR FT-IR spectra of ReTC-MOP before (top) and after the reaction (bottom).

to the MOP and MOF were compared using UV-vis spectrometry. The same number of ReTC units was prepared in each sample of ReTC-MOP and ReTC-MOF, and the corresponding absorptions in the wavelength range from 350 to 550 nm were compared (Fig. 6a). The ReTC units bound to the MOP showed higher absorption than those bound to the MOF, indicating that the discrete cages of ReTC-MOP improved the light absorption in the reaction solution. The stability of ReTC-MOP during photocatalytic CO_2 conversion was characterized using ESI-MS and IR spectroscopy after the reaction. ReTC-MOP samples were collected after 24 h of photocatalysis and washed with methanol to remove impurities. ReTC-MOP generated peaks at *m*/*z* of 895.64, 972.73, 1050.10 and 1126.49, attributed to $[\mathbf{0}]^{4+}$, $[\mathbf{1}]^{4+}$, $[\mathbf{2}]^{4+}$ and $[\mathbf{3}]^{4+}$ species preserved during the reaction (Fig. 6b). This result indicates that ReTC-MOP showed significant structural stability during this prolonged photocatalytic reaction. Moreover, *in situ* ATR FT-IR spectroscopy showed ν(CO) bands at 2022, 1920 and 1910 cm^{-1} with no changes after 30, 60, 90 and 120 min of the reaction. In contrast, these peaks in the H_2ReTC spectra were dramatically reduced in intensity (Fig. S11, ESI†). Even after an extended 24 h reaction, the peaks for the ν(CO) bands were not changed in the case of ReTC-MOP (Fig. 6c). These data demonstrate that ReTC-MOP showed increased structural stability while preserving the molecular conformation of ReTC during the reaction, thus maintaining high photocatalytic CO_2 conversion activity. On this basis, ReTC-MOP evidently shows high photocatalytic activity as a result of the motional freedom of ReTC in the reaction solution (Fig. 4b) and enhanced light absorption (Fig. 6a), while its high stability is due to the structural rigidity of the MOP (Fig. 6b). This rigidity protects the molecular conformation of ReTC from dimerization or decomposition (Fig. 6c). We believe that this approach could be extended to various molecular catalysts to stabilize these compounds without compromising their activity in various targeted catalytic reactions.

Conclusions

ReTC units were chemically bound to discrete cages of MOP and proved highly active and stable during photocatalytic CO_2-to-CO conversion. ReTC-MOP preserved its maximum activity (660 h^{-1} TOF) for up to 24 h, and its cumulative TON of 12 847 was 42.0, 19.6 and 29.3 times those obtained from H_2ReTC, ReTC-MOF(nano) and ReTC-MOF(micro), respectively. The significant activity and stability of ReTC-MOP arise from the high degree of motional freedom, enhanced light absorption and protection of ReTC in the reaction solution.

Nomenclature

MOP	Metal–organic polyhedra
MOF	Metal–organic framework
ReTC	$Re^{I}(CO)_3$(BPYDC)(Cl); a photocatalytic molecule to convert CO_2
BPYDC	2,2′-Bipyridine-5,5′-dicarboxylate; a moiety used to anchor ReTC
H_2ReTC	ReTC without deprotonation of the carboxyl group
CH_2CH_3ReTC	ReTC with an ethyl group on the carboxyl moiety
BPDC	4,4′-Biphenyldicarboxylate comprising the MOP and MOF
BPDC-MOP	MOP composed of six BPDC

BPDC-MOP crystal	A crystal in which BPDC-MOP units are periodically arranged with long-range order
ReTC-MOP	MOP composed of five BPDC and one ReTC on average
BPDC-MOP crystal	A crystal in which ReTC-MOP is periodically arranged with long-range order
ReTC-MOF(nano)	A nanocrystalline MOF containing ReTC
ReTC-MOF(nano)	A microcrystalline MOF containing ReTC
TEA	Trimethylamine
TON	Turnover number
TOF	Turnover frequency.

Conflicts of interest

There are no conflicts to declare.

Acknowledgements

This work was supported by the Basic Science Research Program (NRF-2019R1A2C4069764, 2016R1C1B1010781, and NRF-2019R1C1C1006833) and Next Generation Carbon Upcycling Project (2017M1A2A2046736), which were funded by the Korea Government (MSIP) through the National Research Foundation of Korea (NRF). We especially thank Prof. Wonyoung Choe for his pioneering work and introduction to Zr-based MOP, and Dr Dohyung Kim for his valuable comments.

References

1 W. Kim, B. A. McClure, E. Edri and H. Frei, *Chem. Soc. Rev.*, 2016, **45**, 3221–3243.
2 W. Kim, E. Edri and H. Frei, *Acc. Chem. Res.*, 2016, **49**, 1634–1645.
3 Z. Jiang, H. Sun, T. Wang, B. Wang, W. Wei, H. Li, S. Yuan, T. An, H. Zhao, J. Yu and P. K. Wong, *Energy Envrion. Sci.*, 2018, **11**, 2382–2389.
4 S. Sorcar, Y. Hwang, J. Lee, H. Kim, K. M. Crimes, C. A. Grimes, J.-W. Jung, C.-H. Cho, T. Majima, M. R. Hoffmann and S.-I. In, *Energy Envrion. Sci.*, 2019, **12**, 2685–2696.
5 G. Sahara and O. Ishitani, *Inorg. Chem.*, 2015, **54**, 5096–5104.
6 T. W. Schneider, M. Z. Ertem, J. T. Muckerman and A. M. A-Boza, *ACS Catal.*, 2016, **6**(8), 5473–5481.
7 S. Sato, A. Sekine, Y. Ohashi, O. Ishitani, A. M. Blanco-Rodriguez, A. Vlcek, T. Undo and K. Koike, *Inorg. Chem.*, 2007, **46**(9), 3531–3540.
8 E. E. Benson and C. P. Kubiak, *Chem. Commun.*, 2012, **48**, 7374–7376.
9 Y. Hayashi, S. Kita, B.-S. Brunschwig and E. Fujita, *J. Am. Chem. Soc.*, 2003, **125**, 11976–11987.
10 P. Lang, R. Giereth, S. Tschierlei and M. Schwalbe, *Chem. Commun.*, 2019, **55**, 600–603.
11 B. J. Hare, D. Maiti, Y. A. Daza, V. R. Bhethanabotla and J. N. Kuhn, *ACS Catal.*, 2018, **8**(4), 3021–3029.
12 M. Waki, K. Yamanaka, S. Shirai, Y. Maegawa, Y. Goto, Y. Yamada and S. Inagaki, *Chem. – Eur. J.*, 2018, **24**, 3846–3853.
13 L. C. L. Cao, S. Sahu, P. Anilkumar, C. E. Bunker, J. A. Xu, K. A. S. Fernando, P. Wang, E. A. Guliants, K. N. Tackett and Y. P. Sun, *J. Am. Chem. Soc.*, 2011, **133**, 4754–4757.
14 T.-T. Li, B. Shan and T. J. Meyer, *ACS Energy Lett.*, 2019, **4**(3), 629–636.
15 H. Y. V. Ching, X. Wang, M. He, N. P. Holland, R. Guillot, C. Slim, S. Griveau, H. C. Bertrand, C. Policar, F. Bedioui and M. Fontecave, *Inorg. Chem.*, 2017, **56**(5), 2966–2976.
16 S.-C. Yang, S. H. Pang, T. P. Sulmonetti, W.-N. Su, J.-F. Lee, B.-J. Hwang and C. W. Jones, *ACS Catal.*, 2018, **8**(12), 12056–12066.
17 X. Cui, J. Wang, B. Liu, S. Ling, R. Long and Y. Xiong, *J. Am. Chem. Soc.*, 2018, **140**(48), 16514–16520.
18 A. Aitbekova, L. Wu, C. J. Wrasman, A. Boubnov, A. S. Hoffman, E. D. Goodman, S. R. Bare and M. Cargnello, *J. Am. Chem. Soc.*, 2018, **140**(42), 13736–13745.
19 L. A. Faustino, B. L. Souza, B. N. Nunes, A.-T. Duong, F. Sieland, D. W. Bahnemann and A. O. T. Patrocinio, *ACS Sustainable Chem. Eng.*, 2018, **6**(5), 6073–6083.
20 B. Liu, C. Li, G. Zhang, X. Yao, S. S. C. Chuang and Z. Li, *ACS Catal.*, 2018, **8**(11), 10446–10456.
21 S.-J. Woo, S. Choi, S.-Y. Kim, P. S. Kim, J. H. Jo, C. H. Kim, H.-J. Son, C. Pac and S. O. Kang, *ACS Catal.*, 2019, **9**(3), 2580–2593.
22 H.-Y. Cheong, S.-Y. Kim, Y.-J. Cho, D. W. Cho, C. H. Kim, H.-J. Son, C. Pac and S. O. Kang, *Inorg. Chem.*, 2017, **56**(19), 12042–12053.
23 W. Kim, T. Tachikawa, T. Majima, C. Li, H.-J. Kim and W. Choi, *Energy Environ. Sci.*, 2010, **3**, 1789–1795.
24 C. Wang, Z. Xie, K.-E. DeKrafft and W. Lin, *J. Am. Chem. Soc.*, 2011, **133**, 13445–13454.
25 S. Zhang, L. Li, S. Zhao, Z. Sun and J. Luo, *Inorg. Chem.*, 2015, **54**, 8375–8379.
26 K. M. Choi, D. Kim, B. Rungtaweevoranit, C.-A. Trickett, J. T. D. Barmanbek, A.-S. Alshammari, P. Yang and O. M. Yaghi, *J. Am. Chem. Soc.*, 2017, **139**, 356–362.
27 U. J. Ryu, S. J. Kim, H.-K. Lim, H. Kim, K. M. Choi and J. K. Kang, *Sci. Rep.*, 2017, **7**, 612, DOI: 10.1038/s41598-017-00574-1.
28 L. Li, S. Zhang, L. Xu, J. Wang, L.-X. Shi, Z.-N. Chen, M. Hong and J. Luo, *Chem. Sci.*, 2014, **5**, 3808–3813.
29 S. Zhang, L. Li, S. Zhao, Z. Sun, M. Hong and J. Luo, *J. Mater. Chem. A*, 2015, **3**, 15764–15768.
30 Y. Fu, D. Sun, Y. Chen, R. Huang, Z. Ding, X. Fu and Z. Li, *Angew. Chem., Int. Ed.*, 2012, **51**, 3364–3367.
31 D. Wang, R. Huang, W. Liu, D. Sun and Z. Li, *ACS Catal.*, 2014, **4**, 4254–4260.
32 X. Fang, Q. Shang, Y. Wang, L. Jiao, T. Yao, Y. Li, Q. Zhang, Y. Luo and H.-L. Jiang, *Adv. Mater.*, 2018, **30**(7), 1705112–1705118.
33 P. Wu, X. Guo, L. Cheng, C. He, J. Wang and C. Duan, *Inorg. Chem.*, 2016, **55**, 8153–8159.
34 J. Schneider, K. Q. Vuong, J. A. Calladine, X.-Z. Sun, A. C. Whitwood, M. W. George and R. N. Perutz, *Inorg. Chem.*, 2011, **50**(23), 11877–11889.

35 Q. Yang, C.-C. Yang, C.-H. Lin and H.-L. Jiang, *Angew. Chem., Int. Ed.*, 2019, **58**(11), 3511–3515.
36 J.-D. Xiao and H.-L. Jiang, *Acc. Chem. Res.*, 2019, **52**(2), 356–366.
37 X. Ma, L. Wang, Q. Zhang and H.-L. Jiang, *Angew. Chem., Int. Ed.*, 2019, **58**(35), 12175–12179.
38 C. Gao, J. Wang, H. Xu and Y. Xiong, *Chem. Soc. Rev.*, 2017, **46**, 2799–2823.
39 V. S. Vyas, V. W. Lau and B. V. Lotsch, *Chem. Mater.*, 2016, **28**, 5191–5204.
40 M. Eddaoudi, J. Kim, J. B. Wachter, H. K. Chae, M. O'Keeffe and O. M. Yaghi, *J. Am. Chem. Soc.*, 2001, **123**(18), 4368–4369.
41 D. J. Tranchemontagne, Z. Ni, M. O'Keeffe and O. M. Yaghi, *Angew. Chem., Int. Ed.*, 2008, **47**, 5136–5147.
42 Y.-H. Kang, X.-D. Liu, N. Yan, Y. Jiang, X.-Q. Lin, L.-B. Sun and J.-R. Li, *J. Am. Chem. Soc.*, 2016, **138**(19), 6099–6102.
43 W. Lin, D. Yuan, A. Yakovenko and H.-C. Zhou, *Chem. Commun.*, 2011, **47**, 4968–4970.
44 H. Vardhan and F. Verpoort, *Adv. Synth. Catal.*, 2015, **357**, 1351–1368.
45 M. Sun, Q.-Q. Wang, C. Qin, C.-Y. Sun, X.-L. Wang and Z. M. Su, *Chem. – Eur. J.*, 2019, **25**, 2824–2830.
46 Y. Han, J.-R. Li, Y. Xie and G. Guo, *Chem. Soc. Rev.*, 2014, **43**, 5952–5981.
47 J. Jiao, C. Tan, Z. Li, Y. Liu, X. Han and Y. Cui, *J. Am. Chem. Soc.*, 2018, **140**(6), 2251–2259.
48 D. Nam, J. Huh, J. Lee, J. H. Kwak, H. Y. Jeong, K. Choi and W. Choe, *Chem. Sci.*, 2017, **8**, 7765–7771.
49 G. Liu, Z. Ju, D. Yuan and M. Hong, *Inorg. Chem.*, 2013, **52**, 13815–13817.
50 G. Liu, M. Zeller, K. Su, J. Pang, Z. Ju, D. Yuan and M. Hong, *Chem. – Eur. J.*, 2016, **22**, 17345–17350.

